RSC Advances

PAPER

View Article Online
View Journal | View Issue

Cite this: *RSC Adv.*, 2025, **15**, 41856

Aptamer-conjugated core–shell magnetic nanoparticles for quick and specific separation of gram-negative bacteria

Rakshya Panta,[a] Chao Lu,[b] Howyn Tang [a] and Jin Zhang *[ab]

Received 26th August 2025
Accepted 23rd October 2025

DOI: 10.1039/d5ra06380a

rsc.li/rsc-advances

Quick separation of gram-negative bacteria, such as *Escherichia coli* (*E. coli*), from water sources is crucial for ensuring timely public health protection and promoting environmental sustainability. This study demonstrates that aptamer-conjugated core–shell magnetic nanoparticles (MNPs) can quickly capture *E. coli DH5α* from water. The core–shell MNP composed of an iron (Fe_3O_4) core and a silica (SiO_2) shell has been bio-conjugated with aptamers using glutaraldehyde as a cross-linker. The Fe_3O_4 core has an average diameter of approximately 16 ± 5 nm, and the thickness of the silica shell is around 24 ± 4 nm. Our results show that 1 mg mL^{-1} of the Aptamer-Fe_3O_4@SiO_2 nanoparticles (NPs) can efficiently capture and remove *E. coli DH5α* cells (1×10^7 CFU mL^{-1}) from aqueous solutions in just 5 minutes when subjected to an external magnetic field of 2.0 kOe. The selective interaction between *E. coli DH5α* and the Aptamer-Fe_3O_4@SiO_2 NPs has been analyzed as compared to the interaction between the Aptamer-Fe_3O_4@SiO_2 NPs and different strains of *E. coli* and gram-positive bacteria. This work demonstrates that the conjugation of aptamers on Fe_3O_4@SiO_2 NPs is a powerful tool for fast bacterial detection and magnetic isolation, supporting future use in monitoring water quality and protecting public health.

1. Introduction

Gram-negative bacteria in natural water bodies often indicate fecal contamination.[1] Their presence can degrade water quality and aquatic ecosystems. In addition, gram-negative bacteria can easily form biofilms that clog pipes, reduce water flow, and facilitate the persistence and spread of pathogens.[2,3] On the other hand, many gram-negative bacteria, such as *Escherichia coli* (*E. coli*), are multidrug-resistant (MDR), including ESBL-producing and carbapenem-resistant strains, making timely detection critical for patient survival and infection control.[4] *E. coli* is the most common gram-negative bacterium in the human gastrointestinal tract and often lacks virulence in this setting. However, when found outside the intestinal tract, it causes urinary tract infections (UTI), peritonitis, pneumonia, and bacteraemia.[5] Though different methods have been developed to separate bacteria; it is still challenging to specifically identify and separate certain strains of bacteria. It is noted that existing methods for identifying bacteria, like enzyme-linked immunosorbent assay (ELISA) and polymerase chain reaction (PCR), are often time-consuming and require multiple days to yield results.[6] Therefore, a new cost-effective system is required to quickly and specifically capture and separate a certain strain of *E. coli* from water.

It is noted that nanoparticles (NPs) with a diameter in the range of 1–100 nm can be taken up passively by eukaryotic cells to aid in tracking cells or drug delivery.[7,8] Penetrating the cell wall of bacteria by these nanostructures is limited to those with a diameter of less than 5 nm.[9] Engineered magnetic nanoparticles (MNPs) have demonstrated the capability for bioseparation of bioproducts, including cells and nucleic acids.[10–12] Consequently, surface modifications are essential to optimize the interaction between NPs and bacteria interaction.[13]

Recently, MNPs conjugated with different receptors have demonstrated the ability to capture bacteria. Xu and his colleagues used vancomycin-conjugated Fe-based magnetic nanoparticles to bind with the peptide and capture *E. coli* at a low 3×10^4 cells per ml concentration.[14] It has been seen that antimicrobial peptides, such as bacitracin A, pediocin, and cecropin, functionalized MNPs are applied as probes for bacterial capture, isolation, and enrichment.[15] El-Boubbou and colleagues attached lectin to MNPs and used mannose to bind to, capture, and eliminate *E. coli*.[16]

Aptamers are short single-stranded oligonucleotides (2–25 kDa) that can fold into specific three-dimensional shapes, allowing them to bind tightly and selectively to target molecules or structures on the surface of bacteria.[17,18] DNA aptamers have been bio-conjugated to optical NPs to detect *Staphylococcus aureus* (*S. aureus*) and *E. coli*.[19–21] Specifically, aptamer 8.28A has a dissociation constant (K_d) of 27.4 ± 18.7 nM for *E. coli DH5α*,

[a]*School of Biomedical Engineering, University of Western Ontario, London, Ontario, N6A 5B9, Canada. E-mail: jzhang@eng.uwo.ca*

[b]*Department of Chemical and Biochemical Engineering, University of Western Ontario, London, Ontario, N6A 5B9, Canada*

demonstrating sufficient binding affinity and specificity for efficient bacterial capture.[22] The conjugation of aptamers to NPs can efficiently improve the selective separation of bacteria from water.[23,24] However, direct bioconjugation of aptamers on MNPs could cause the unexpected demagnetization due to the oxidation of MNPs. Previous studies in core–shell MNPs demonstrated that the silica (SiO_2) shell can prevent the oxidation of the magnetic core, and the fluorophore-loaded mesoporous SiO_2 nanostructures have 20 times more brightness than that of semiconductor quantum dots.[25] Recent reports have further highlighted the versatility of silica-coated MNPs in biomedical applications, including bacterial capture, drug delivery, and biosensing, demonstrating their efficiency in complex biological systems.[26–28]

In this paper, core–shell MNPs made of a Fe_3O_4 core and a SiO_2 shell have been produced, following the bioconjugation of an aptamer which can specifically bind to *E. coli DH5α*. The performance of the aptamer-bioconjugated on the core–shell MNPs, *i.e.* Aptamer-Fe_3O_4@SiO_2 NPs, applied for quickly and selectively separate *E. coli DH5α* from water has been investigated.

2. Materials and experimental

The aptamer used in this study was purchased from Integrated DNA Technologies. The sequence of the aptamer was aptamer (8.28A), 5-NH_2-(CH_2)6-TCC TCG CGT TTG GAT TCA TGT TGG TTT GTC GGT GTA TTG T-3, which has a specific binding to *E. coli* (*DH5a*). The following analytical-grade chemicals were obtained from Sigma-Aldrich: cetyltrimethylammonium bromide (CTAB, 98%), toluene, ammonium hydroxide solution (NH_4OH, 28%), iron(II) chloride ($FeCl_2$, 98%), iron(III) chloride ($FeCl_3$, 97%), sodium hydroxide (NaOH, 97%), fluorescein isothiocyanate isomer (FITC, 90%), tetraethyl orthosilicate (TEOS, 98%), aminopropyltriethoxysilane (APTS, 98%), and glutaraldehyde (Glu, Grade I, 25%).

2.1. Synthesis of core–shell MNPs

The core–shell MNPs, *i.e.*, Fe_3O_4@SiO_2 NPs, were produced based on previous reports.[29,30] Fe_3O_4 NPs were produced *via* the heat decomposition method.[11,31] First, 2 mM of $FeCl_3 \cdot 6H_2O$ was mixed with ethanol, hexane, and oleic acid, and stirred at room temperature for 30 minutes. Next, NaOH was added to the mixture within a closed vessel and stirred for 4 hours at 70 °C. After the reaction, the solution was separated into two layers and dried. The dried layers were heated overnight at 80 °C to evaporate the hexane, yielding a sticky Fe(oleate)$_3$ precursor. This precursor was subsequently dispersed in oleic acid along with 12.5 mL of 1-octadecene. The mixture was purged using nitrogen gas for 30 minutes at room temperature, then heated to 320 °C for 30 minutes under the protection of nitrogen gas. After heating, the mixture was allowed to cool to room temperature, and the nanoparticles were collected through centrifugation.

200 μL of the above Fe_3O_4 NPs was mixed with 20 mL of cyclohexane and stirred for 15 minutes. Afterward, 750 μL of surfactant was added, and the mixture was stirred for an additional 30 minutes. Ammonium was then introduced, and the solution was stirred for another 30 minutes. Following this, the mixture was allowed to stir for 24 hours. Subsequently, 15 μL of aminopropyltriethoxysilane (APTS) was added to the solution and mixed for a duration of 24 to 36 hours. Finally, the core–shell nanoparticles were centrifuged, subjected to ultrasonic mixing, and stored in ethanol for later use.

2.2. Bioconjugation of aptamer to core–shell MNPs

1 mL (0.33 mg mL^{-1}) of the Fe_3O_4@SiO_2 NPs reacted with 200 μL of glutaraldehyde solution (0.0025%) for one hour to activate the surface for the bioconjugation. Following that, 3 μl (100 μM) of aptamer (8.28A) was added to the mixture and allowed to react for an additional two hours to facilitate the bioconjugation process. Aptamer (8.28A), 5-NH_2-(CH_2)6-TCC TCG CGT TTG GAT TCA TGT TGG TTT GTC GGT GTA TTG T-3 has a specific binding to *E. coli* (*DH5a*).[22] The conjugation efficiency of aptamer 8.28A to Fe_3O_4@SiO_2 NPs was determined by measuring the UV absorbance at 260 nm. A calibration curve was prepared using known concentrations of the aptamer (0.0195–1.25 μM) and their corresponding absorbances. After the bioconjugation reaction, the nanoparticles were magnetically separated, and the absorbance of the unbound aptamer in the supernatant was measured. The core–shell MNPs, referred to as Aptamer-Fe_3O_4@SiO_2 NPs in this paper, are the focus of this study.

2.3. Capture of *E. coli* (*DH5α*) by using aptamer-Fe_3O_4@SiO_2 NPs

Non-pathogenic *E. coli DH5α* was grown at 37 °C for 24 hours in broth media. The optical density (OD) of the culture was adjusted to a concentration of approximately 10^7 CFU mL^{-1}. The cultures were diluted 10^{-3} in phosphate-buffered saline (PBS, 0.01 M, pH 7.4). Aptamer-conjugated Fe_3O_4@SiO_2 magnetic nanoparticles (Aptamer-Fe_3O_4@SiO_2 NPs) were washed with sterilized PBS (0.01 M, pH 7.4) and added to 1 mL of each diluted bacterial suspension. After thorough mixing and incubation, magnetic separation was performed to isolate the Aptamer-Fe_3O_4@SiO_2 NPs-bound bacteria. The supernatants were collected at 5- and 10-minute post-separation and plated on LB agar to determine the number of unbound bacteria by colony formation assay. The same procedure was applied to *E. coli BL21* and *S. aureus* to assess the specificity of the Aptamer-Fe_3O_4@SiO_2 NPs. The response of *E. coli DH5a* to the Aptamer-Fe_3O_4@SiO_2 NPs was further evaluated by comparing it to the response of *E. coli* to negative control samples using standard Fe_3O_4@SiO_2 NPs.

To evaluate the bacterial capture efficiency of Aptamer-Fe_3O_4@SiO_2 NPs compared to Fe_3O_4@SiO_2 NPs without aptamer conjugation, the stock suspension with 4.5×10^7 CFU mL^{-1} and the diluted suspension with 3×10^6 CFU mL^{-1} were produced. 200 μL of Aptamer-Fe_3O_4@SiO_2 NPs or 200 μL of non-conjugated Fe_3O_4@SiO_2 NPs (control) with the same concentration was added, followed by magnetic separation, which was performed to isolate nanoparticles bound to bacteria. The

remaining supernatant was collected and the concentration of that was determined by serial dilution method. Four replicates were prepared for each dilution.

2.4. Characterization of nanostructures

The magnetic characteristics of the samples were assessed using a vibrating sample magnetometer (VSM, Lakeshore 7407), with a measurement range of 10^7 to 10^3 emu and a field accuracy of ±0.05% of full scale. Transmission electron microscopy (TEM) was employed to investigate the core–shell structure and validate the interaction between the bacteria and the nanoparticles, utilizing a Philips CM-10 TEM operating at 100 kV. Additionally, Fourier transform infrared (FTIR) spectroscopy (Cary 630, Agilent) and electrophoresis were conducted to analyze the bioconjugation of aptamer (8.28A) to MNPs.

3. Results and discussion

3.1. Synthesis and characterization of core–shell MNPs

The core–shell MNPs consist of a Fe_3O_4 core encapsulated within a silica shell. Fig. 1 shows the TEM micrographs of core–shell MNPs, *i.e.*, Fe_3O_4@SiO_2 NPs. The average diameter of the core–shell MNPs is estimated at 40 ± 9 nm, and the Fe_3O_4 NPs are estimated at 16 ± 5 nm. The distinct boundary between the core and the shell can be observed. The thickness of the SiO_2 shell is around 24 ± 4 nm.

Furthermore, the magnetic properties of Fe_3O_4 NPs and core–shell MNPs, *i.e.*, Fe_3O_4@SiO_2 NPs, have been investigated under VSM. Fig. 2 shows the hysteresis loops of Fe_3O_4 NPs and Fe_3O_4@SiO_2 NPs measured by VSM. Both Fe_3O_4 NPs and Fe_3O_4@SiO_2 NPs show superparamagnetic properties as their coercivity (H_c) and remanence (M_r) are essentially zero, as shown in the inset graph of Fig. 2. The Fe_3O_4 nanoparticles exhibited a saturation magnetization (M_s) of approximately 57 emu g^{-1} when the magnetic field is 12 kOe. In contrast, the Fe_3O_4@SiO_2 NPs showed a reduced value of around 38 emu g^{-1}, representing an approximate 33% decline. This decrease is attributed to the non-magnetic nature of the silica shell, which lowers the overall magnetic signal. Nevertheless, the Fe_3O_4@SiO_2 NPs retain sufficient magnetic responsiveness, making them suitable for applications that require magnetic separation and precise control, including biosensing, drug delivery, and magnetic resonance imaging.

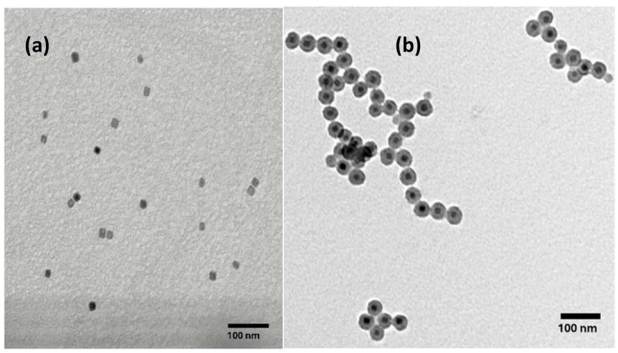

Fig. 1 (a) TEM micrographs of (a) Fe_3O_4 NPs, (b) Fe_3O_4@SiO_2 NPs.

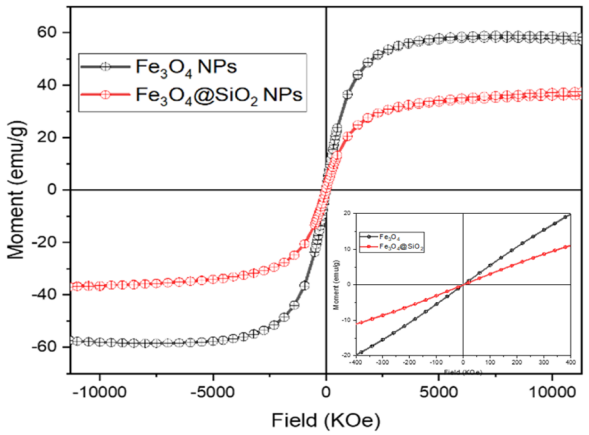

Fig. 2 Hysteresis loops of Fe_3O_4 NPs, and Fe_3O_4@SiO_2 NPs.

3.2. Analysis of the bioconjugation of aptamer to core–shell MNPs

FTIR has been applied to investigate three samples: amino-modified aptamer (8.28A), Fe_3O_4@SiO_2 NPs, and Aptamer-Fe_3O_4@SiO_2 NPs as shown in Fig. 3. For the sample of aptamer, the band at 3220 cm^{-1} is attributed to –N–H bending vibration which confirmed the modification the amino group at the 5′ end.[32] In addition, the bands between 1800 and 1500 cm^{-1} is related to the stretching vibrations of double bonds in the base planes; and the bands between 1250 and 1000 cm^{-1} are related to vibration of the phosphate groups.[33,34] The Si–O–Si stretching vibration peak observed near 1100 cm^{-1} indicates the presence of the silica shell in the core–shell nanoparticles. Furthermore, a –C=O stretching peak at 1760 cm^{-1} is observed in the spectrum of the free amino-modified aptamer but is absent in the conjugated nanoparticles, suggesting that the aldehyde groups were utilized during the conjugation. To the sample of Fe_3O_4@SiO_2 NPs in an aqueous medium, the –O–H vibration can

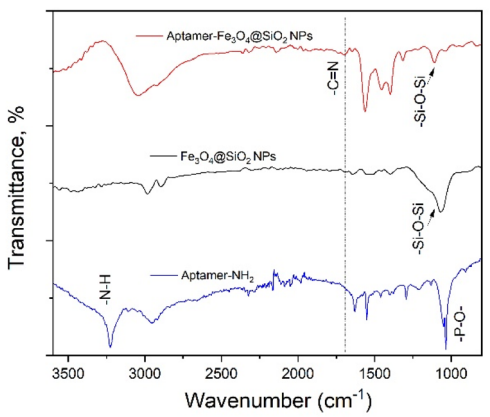

Fig. 3 FTIR spectra of Fe_3O_4@SiO_2 NPs, amino modified aptamer (8.28A), and Aptamer-Fe_3O_4@SiO_2 NPs.

be observed at 3400 cm^{-1}. The formation of carbon–nitrogen double bonds (–C═N) at 1690 cm^{-1}, known as Schiff bases,[35] in a sample of Aptamer-Fe_3O_4@SiO_2 NPs, confirms the bioconjugation of aptamer to Fe_3O_4@SiO_2 NPs *via* the cross-linking reaction using glutaraldehyde.

To further verify the bioconjugation of the aptamer to Fe_3O_4@SiO_2 NPs, gel electrophoresis was conducted using a 1% agarose gel, running at 100 V for 45 minutes.

The resulting gel analysis, shown in Fig. 4, displays three distinct bands: Lane 1 refers to free aptamer; Lane 2 is the sample of Aptamer-Fe_3O_4@SiO_2 NPs; Lane 3 is Fe_3O_4@SiO_2 NPs alone. Lane 1 illustrates the significant migration of the free aptamer from the negative electrode to the positive electrode, driven by its negative charge. The Fe_3O_4@SiO_2 NPs in Lane 3 stay at the top with a tail exhibiting minimal migration due to their larger size and lack of negative charge on the surface. The Aptamer-Fe_3O_4@SiO_2 NPs in Lane 2 migrate more slowly compared to the free aptamer in Lane 1, but much quicker than the Fe_3O_4@SiO_2 NPs in Lane 3, indicating successful bioconjugation of the aptamer to the core–shell MNPs, as the negatively charged aptamer helps the migration of the conjugated core–shell MNPs; however, the large molecular size of the Aptamer-Fe_3O_4@SiO_2 NPs causes the lower migration as compared to the free aptamer. Using a calibration curve of aptamer 8.28A absorbance at 260 nm (Fig. S1, SI), the concentration of unbound aptamer in the supernatant after magnetic separation was determined, indicating that approximately 32% of the aptamer was successfully conjugated to the Fe_3O_4@SiO_2 nanoparticles (Fig. 5).

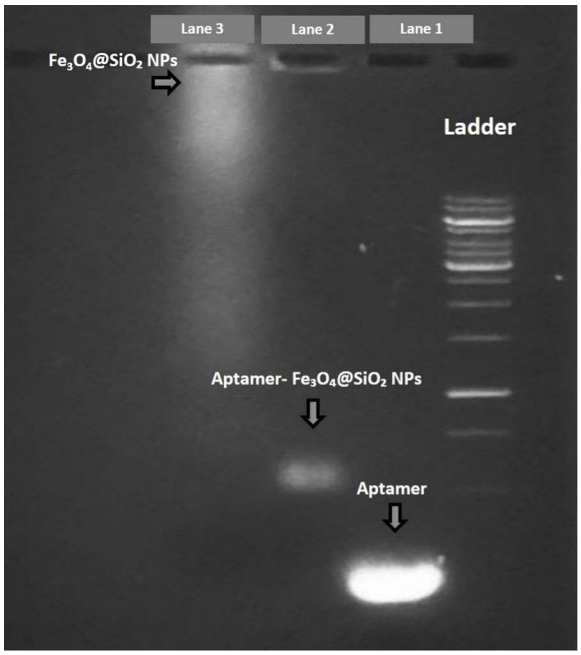

Fig. 4 Gel electrophoresis applied to investigate the bioconjugation of Aptamer to Fe_3O_4 @SiO_2 NPs. Lane 1: Aptamer; Lane 2: Aptamer-Fe_3O_4@SiO_2 NPs; Lane 3, Fe_3O_4@SiO_2 NPs.

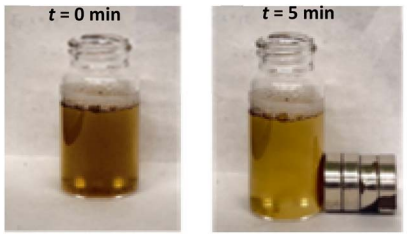

Fig. 5 Photos of *E. coli DH5α* suspension (1×10^7 CFU mL^{-1}) before (t = 0 min) and after being captured by 1 mg Fe_3O_4@SiO_2 NPs under an external magnetic field, 2.0 kOe within 5 min (right).

3.3. Targeted recognition and separation of *E. coli DH5α*

Our results indicate that Aptamer-Fe_3O_4@SiO_2 NPs (1 mg) can effectively capture and remove *E. coli DH5α* cells at a concentration of 1×10^7 CFU mL^{-1} from a 10 mL solution when subjected to an external magnetic field of 2.0 kOe. This selective capture is consistent with the high binding affinity of aptamer 8.28A to *E. coli DH5α*, which has a dissociation constant (K_d) of 27.4 ± 18.7 nM,[22] confirming that the aptamer can efficiently recognize and bind to the target strain. The same procedure was applied to *S. aureus* to assess the specificity of the Aptamer-Fe_3O_4@SiO_2 NPs. For *S. aureus*, both bioconjugated and non-bioconjugated nanoparticles were tested to compare capture efficiency, enabling a direct comparison with *DH5α*. The bacterial removal efficiency reached approximately 66.7% within 5 minutes and achieved complete (100%) removal within 10 minutes under an external magnetic field of 2.0 kOe. This result highlights the high binding affinity and fast magnetic separation efficiency of the Aptamer-Fe_3O_4@SiO_2 NPs compared with controls.

The supernatants after magnetic separation were collected when separation time at t = 5 and 10 minutes, respectively; and the samples were cultured on an agar plate to determine the number of unbound bacteria as shown in Fig. 6. *E. coli DH5α* sample exhibited very few colonies, approximately three colonies at t = 5 minutes; and nearly absent at t = 10 minutes. In contrast, *E. coli BL21* and *S. aureus* showed no noticeable change in colony formation across the same time points. The bacterial removal (separation) efficiency of Aptamer-Fe_3O_4@SiO_2 NPs against different bacteria with t is presented in Fig. 7. 1 mg Aptamer-Fe_3O_4@SiO_2 NPs can remove all *E. coli DH5α* cells at

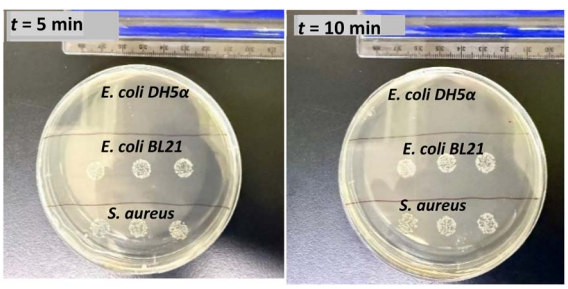

Fig. 6 Supernatants collected at t = 5 and t = 10 min showed few or no *E. coli DH5α* colonies, while *E. coli BL21* and *S. aureus* remained unaffected.

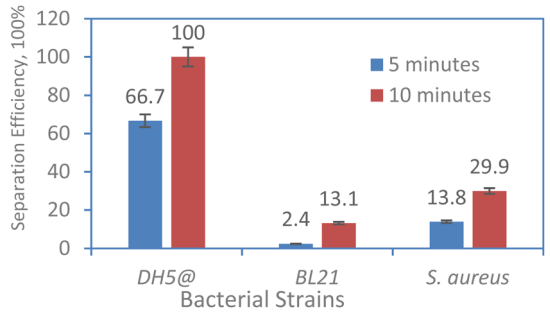

Fig. 7 Selective bacterial separation efficiency of Aptamer-Fe_3O_4@-SiO_2 NPs at 5 and 10 minutes, respectively. Error bars represent the standard deviation from triplicates.

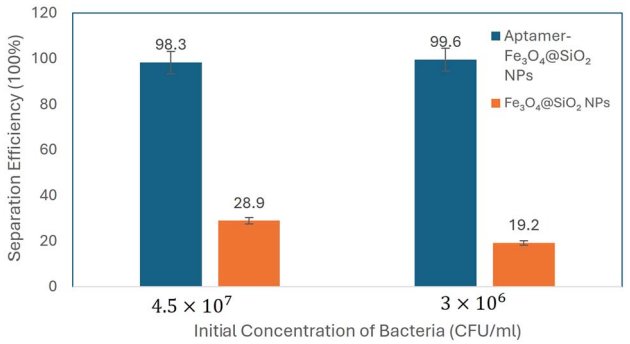

Fig. 8 Living *E. coli DH5α* after 10 minutes of magnetic separation with aptamer-MNPs and MNPs at 0.1× and 0.01× dilutions. The control is core–shell MNPs without aptamer. Bars represent the mean of four replicates.

a concentration of 1×10^7 CFU mL^{-1} from a 10 mL solution when $t = 10$ minutes. However, the separation efficiency of Aptamer-Fe_3O_4@SiO_2 NPs against *E. coli BL21* and *S. aureus* is 13.1 % and 29.9%, respectively, when $t = 10$ minutes.

The bacterial removal efficiency of Aptamer-Fe_3O_4@SiO_2 NPs was further investigated with the control (Fe_3O_4@SiO_2 NPs without aptamer) to assess the affinity of aptamer to *E. coli DH5α*. As shown in Fig. 8, Aptamer-Fe_3O_4@SiO_2 can remove 98.3% of bacteria at 4.5×10^7 CFU mL^{-1}, while less that 28.9% of bacteria can be removed when it was treated with MNPs without the conjugation of aptamer. To diluted solution at 3×10^6 CFU mL^{-1}, removal by Aptamer-Fe_3O_4@SiO_2 remained high at 99.6%, whereas Fe_3O_4@SiO_2 can only separate only 19.2% of bacteria. These results demonstrate that the Aptamer-Fe_3O_4@SiO_2 nanoparticles exhibit consistently high and specific bacterial capture, attributed to the strong affinity between the aptamer and the target bacteria. In contrast, the control (non-conjugated Fe_3O_4@SiO_2 MNPs) show limited removal efficiency, likely due to nonspecific physical interactions or gravitational settling. Representative agar plates are shown in Fig. S3 (SI).

4. Conclusion

In conclusion, the engineered MNPs, consist of a Fe_3O_4 core with an average diameter of 16 ± 5 nm, and the silica shell with a thickness of 24 ± 4 nm. The core–shell MNPs were successfully bio-conjugated with aptamer (8.28A) using glutaraldehyde as a cross-linking agent. This study demonstrates the effectiveness of Aptamer-Fe_3O_4@SiO_2 NPs in capturing *E. coli DH5α*, a common Gram-negative bacterium, from liquid environments. Our findings reveal that 1 mg mL^{-1} of these Aptamer-Fe_3O_4@SiO_2 NPs can efficiently capture and remove about 66.7% of *E. coli DH5a* cells (1×10^7 CFU mL^{-1}) from solution in 5 min under an external magnetic field of 2.0 kOe; when $t =$ 10 min, no viable bacteria remain in the solution. Whereas the other strain of *E. coli* cells, *E. coli BL21* and Gram-positive bacterium, *S. aureus* could not be effectively removed by the Aptamer-Fe_3O_4@SiO_2 NPs under the same condition. The effective bacteria capture of Aptamer-Fe_3O_4@SiO_2 NPs is further verified as compared to the capture capability of core–shell MNPs without the conjugation of aptamer. These findings indicate that Aptamer-Fe_3O_4@SiO_2 NPs can selectively bind to and remove *E. coli DH5α*, confirming both the successful conjugation of aptamers and the specific recognition of the target strain. This study suggests that Aptamer-Fe_3O_4@SiO_2 are promising method for rapid bacterial detection and magnetic separation, with potential applications in environmental monitoring and public health.

Author contributions

Rakshya Panta: investigation, validation, methodology, formal analysis, writing – original draft. Chao Lu: investigation, validation. Howyn Tang: investigation, validation. Jin Zhang: conceptualization, methodology, funding acquisition supervision, writing – review & editing. All authors have given approval to the final version of the manuscript.

Conflicts of interest

The authors have no conflicts of interest/competing interests to declare.

Data availability

Research data are available as per request.

Supplementary information: S1 – absorbance of Aptamer 8.28A at 260 nm; S2 – bacterial colony morphology. See DOI: **https://doi.org/10.1039/d5ra06380a**.

Acknowledgements

We are thankful for the financially support from Natural Sciences and Engineering Research Council of Canada (NSERC).

References

1 D. A. Holcomb and J. R. Stewart, *Curr. Environ. Health Rep.*, 2020, 7, 311–324.
2 R. Azari, M. H. Yousefi, A. A. Fallah, A. Alimohammadi, N. Nikjoo, J. Wagemans, E. Berizi, S. Hosseinzadeh, M. Ghasemi and A. M. Khaneghah, *Biofilm*, 2024, 7, 100170.

3 E. Gall, A. Long and K. K. Hall, in *Making Healthcare Safer III: A Critical Analysis of Existing and Emerging Patient Safety Practices*, Agency for Healthcare Research and Quality, US, 2020.
4 Z. D. Blount, *elife*, 2015, **4**, e05826.
5 J. D. McCue, *J. Am. Geriatr. Soc.*, 1987, **35**, 213–218.
6 G. Acharya, C.-L. Chang and C. Savran, *J. Am. Chem. Soc.*, 2006, **128**, 3862–3863.
7 N. Hoshyar, S. Gray, H. Han and G. Bao, *Nanomedicine*, 2016, **11**, 673–692.
8 J. Zhang, L.-M. Postovit, D. Wang, R. B. Gardiner, R. Harris, M. Abdul and A. Thomas, *Nanoscale Res. Lett.*, 2009, **4**, 1297.
9 N. Białas, V. Sokolova, S. B. van der Meer, T. Knuschke, T. Ruks, K. Klein, A. M. Westendorf and M. Epple, *Nano Sel.*, 2022, **3**, 1407–1420.
10 J. Hong, L. Wang, Q. Zheng, C. Cai, X. Yang and Z. Liao, *Materials*, 2024, **17**, 2870.
11 L. Chen, F. S. Razavi, A. Mumin, X. Guo, T.-K. Sham and J. Zhang, *RSC Adv.*, 2013, **3**, 2390–2397.
12 L. Yi, Y. Huang, T. Wu and J. Wu, *Neural Regener. Res.*, 2013, **8**, 3036–3046.
13 I. A. Worms, J. Boltzman, M. Garcia and V. I. Slaveykova, *Environ. Pollut.*, 2012, **167**, 27–33.
14 J. Huang, W. Li, X. Bai, F. Xiao and H. Xu, *Coord. Chem. Rev.*, 2023, **488**, 215160.
15 M. D. Adhikari, S. Mukherjee, J. Saikia, G. Das and A. Ramesh, *J. Mater. Chem. B*, 2014, **2**, 1432–1438.
16 K. El-Boubbou, C. Gruden and X. Huang, *J. Am. Chem. Soc.*, 2007, **129**, 13392–13393.
17 J. Zhou and J. Rossi, *Nat. Rev. Drug Discovery*, 2017, **16**, 181–202.
18 X. Zhao, C. Lu, S. Yang and J. Zhang, *Mater. Lett.*, 2020, **264**, 127330.
19 H. N. Abdelhamid and H.-F. Wu, *Spectrochim. Acta, Part A*, 2018, **188**, 50–56.
20 H. Li, W. Ahmad, Y. Rong, Q. Chen, M. Zuo, Q. Ouyang and Z. Guo, *Food Control*, 2020, **107**, 106761.
21 X. Zhao, L. R. Hilliard, S. J. Mechery, Y. Wang, R. P. Bagwe, S. Jin and W. Tan, *Proc. Natl. Acad. Sci. U. S. A.*, 2004, **101**, 15027–15032.
22 M. Renders, E. Miller, C. H. Lam and D. M. Perrin, *Org. Biomol. Chem.*, 2017, **15**, 1980–1989.
23 G. Singh, P. Vajpayee, N. Rani, A. Jyoti, K. C. Gupta and R. Shanker, *Ecotoxicol. Environ. Saf.*, 2012, **78**, 320–326.
24 Z. Herazo-Romero, W. Y. Royero-Bermeo, M. O. Pérez-Navarro, M. M. Sánchez-Jiménez and J. D. Ospina-Villa, *Environments*, 2025, **12**, 329.
25 A. A. Burns, J. Vider, H. Ow, E. Herz, O. Penate-Medina, M. Baumgart, S. M. Larson, U. Wiesner and M. Bradbury, *Nano Lett.*, 2009, **9**, 442–448.
26 R. Fiedler, G. Sivakumaran, J. Mallén and M. Linden, *Chem. Mater.*, 2024, **36**, 2790–2798.
27 H.-M. Kim, D.-M. Kim, C. Jeong, S. Y. Park, M. G. Cha, Y. Ha, D. Jang, S. Kyeong, X.-H. Pham and E. Hahm, *Sci. Rep.*, 2018, **8**, 13938.
28 I. Monaco, P. Armanetti, E. Locatelli, A. Flori, M. Maturi, S. Del Turco, L. Menichetti and M. C. Franchini, *J. Mater. Chem. B*, 2018, **6**, 2993–2999.
29 L. Chen, S. Yang, M. Dotzert, C. J. Melling and J. Zhang, *J. Mater. Chem. B*, 2023, **11**, 998–1007.
30 R. A. Perez, K. D. Patel and H.-W. Kim, *RSC Adv.*, 2015, **5**, 13411–13419.
31 J. Kim, H. S. Kim, N. Lee, T. Kim, H. Kim, T. Yu, I. C. Song, W. K. Moon and T. Hyeon, *Angew. Chem.*, 2008, **47**, 8438–8441.
32 Z. H. Wang, Z. Y. Wang, C. S. Sun, C. Y. Wang, T. Y. Jiang and S. L. Wang, *Biomaterials*, 2010, **31**, 908–915.
33 E. Taillandier and J. Liquier, *Methods Enzymol.*, 1992, **211**, 307–335.
34 J. Dong, Y. Zhang, L. Liu, X. Zhang, L. Li, G. Liu, H. Li, P. Yan and J. Xia, *Chem. Commun.*, 2025, **61**, 7125–7128.
35 T. Akitsu, *Schiff Base in Organic, Inorganic and Physical Chemistry*, BoD – Books on Demand, 2023.